

# A Prediction model of relativistic electrons at geostationary orbit using the EMD-LSTM network and geomagnetic indexes

Hua Zhang<sup>1</sup>, Haoran Xu<sup>1</sup>, GuangShuai Peng<sup>2</sup>, Ye dong Qian<sup>3</sup>, Chao Shen<sup>4</sup>, Zheng Li<sup>2</sup>, Jianwei Yang<sup>3</sup>, and Fang He<sup>5</sup>

<sup>1</sup>Institute of Space Weather, Nanjing University of Information Science & Technology

<sup>2</sup>Nanjing University of Information Science & Technology

<sup>3</sup>Najing university of Information Science & Technology

<sup>4</sup>School of Science, Harbin Institute of Technology

<sup>5</sup>Polar Research Institute of China

November 26, 2022

## Abstract

In this study, We construct the EMD-LSTM model, combined the Empirical Mode Decomposition algorithm (EMD) and the Long Short Term Memory neural network (LSTM), to predict the variation of the >2MeV electron fluxes. The Pc5 power and related geomagnetic indexes as input parameters are used to predict the >2MeV electron fluxes. Compared the prediction results of the model with other classical prediction models, the results shows that the one-day ahead prediction efficiency of the > 2MeV electron fluxes is above 0.80, and the highest prediction efficiency can reach 0.92 in 2011-2013, which is much better than the prediction result of classical prediction models. Selected two high-energy electron flux storm events to verify, the results indicates that the performance of the EMD-LSTM model in the period of the high-energy electron flux storm is also relatively good, especially for the prediction of high-energy electron fluxes at extreme points, and the prediction is closer to actual observation.

# 1 **A Prediction model of relativistic electrons at geostationary orbit**

## 2 **using the EMD-LSTM network and geomagnetic indexes**

3 H. Zhang<sup>1</sup> H. R. Xu<sup>1</sup> G.S. Peng<sup>1</sup> Y. D. Qian<sup>1</sup> C. Shen<sup>2</sup> Z. Li<sup>1</sup> J. W. Yang<sup>1</sup> F. He<sup>3</sup>

4 <sup>1</sup>Institute of Space Weather, Nanjing University of Information Science & Technology,  
5 Nanjing, China.

6 <sup>2</sup>Harbin Institute of Technology, Shen Zhen, China.

7 <sup>3</sup>NMR Key laboratory for Polar Science, Polar Research Institute of China, Shang Hai,  
8 China.

9 *Corresponding author: Hua Zhang (289534957@qq.com)*

### 10 **Key Points:**

- 11 ● Propose a prediction model of relativistic electrons using a deep learning algorithm,  
12 the EMD-LSTM model, to predict the >2MeV electron fluxes.
- 13 ● Use the ultralow frequency Pc5 power and related geomagnetic indexes as input  
14 parameters to predict the >2MeV electron fluxes.
- 15 ● The accuracy of storm-time forecasting is greatly improved, especially few time offset of  
16 between the observation value and the forecast value at the inflection point of lowest  
17 flux.

### 18 **Abstract:**

19 In this study, We construct the EMD-LSTM model, combined the Empirical Mode  
20 Decomposition algorithm (EMD) and the Long Short Term Memory neural network (LSTM),  
21 to predict the variation of the >2MeV electron fluxes. The Pc5 power and related geomagnetic  
22 indexes as input parameters are used to predict the >2MeV electron fluxes. Compared the  
23 prediction results of the model with other classical prediction models, the results shows that  
24 the one-day ahead prediction efficiency of the > 2MeV electron fluxes is above 0.80, and the  
25 highest prediction efficiency can reach 0.92 in 2011-2013, which is much better than the  
26 prediction result of classical prediction models. Selected two high-energy electron flux storm  
27 events to verify, the results indicates that the performance of the EMD-LSTM model in the  
28 period of the high-energy electron flux storm is also relatively good, especially for the

29 prediction of high-energy electron fluxes at extreme points, and the prediction is closer to  
30 actual observation.

### 31 **Plain Language Summary:**

32 During the recovery of a magnetic storm, the relativistic electron fluxes at MeV energy from  
33 the outer radiation belt will be enhanced at geosynchronous orbit. In particular, the >2MeV  
34 electrons could penetrate the surface of satellites and accumulate inside. After a long period,  
35 the effect of such electron fluxes could result in satellites to be unable to operate or to be  
36 damaged completely. A new neural network, called EMD-LSTM, is established by  
37 combination of the EMD and the LSTM, which can process the influence of non-stationary  
38 and long term non-linear of data series. The prediction results of the EMD-LSTM model is  
39 also excellent in dramatic change of data series, and particularly the extreme points of data  
40 series is accurately predicted, and few time offset.

## 41 **1. Introduction**

42 The Geosynchronous orbit (GEO) is located in the region of the outer radiation belt which  
43 distributes generous relativistic electrons. At the same time, hundreds of satellites operate in  
44 this region. During recovery phase of a magnetic storm period, the relativistic electrons rise in  
45 count from 10 up to  $10^5$  (electrons  $\text{Sr}^{-1} \text{s}^{-1}$ ) (Sakaguchi et al., 2013). The deep-dielectric  
46 charging by relativistic electrons could damage satellites at GEO and pose a risk for space  
47 security (Wrenn et al., 2002). According to the statistics of faults, more than fifty failures of  
48 GEO satellites are caused by the accumulation of high-energy charged particles occurred from  
49 March 1992 to April 1994 (He et al., 2013). Therefore, the prediction of >2 MeV electron  
50 fluxes has important scientific and application value, which is the necessary measure to be  
51 taken in advance to reduce the harm of relativistic electrons to space instruments.

52 The sudden acceleration of relativistic electrons is responsible for the increase in fluxes.  
53 At present, two types of acceleration mechanism of relativistic electrons have been proposed:  
54 the mechanism of radial diffusion (Li et al., 2001) and the local interaction of wave-particle  
55 (Simms et al., 2018). Based on the radial diffusion mechanism, Li et al. (2001) proposed a  
56 radial diffusion model that takes solar wind parameters and the interplanetary magnetic field  
57 as input parameters to predict the relativistic electron fluxes of the 1-2 day ahead. The

58 prediction efficiency (PE) of the radial diffusion model is up to 0.64, however, that is not  
59 ideal during the solar maximum period. Turner & Li (2008) developed the LOW-E model,  
60 which uses the low-energy electron fluxes as an input parameter to predict the relativistic  
61 electron fluxes of the 1 day ahead, and the PE of that is up to 0.73. The Space Weather  
62 Prediction Center of the National Oceanic and Atmospheric Administration (NOAA), USA,  
63 developed a prediction model of relativistic electron fluxes (REFM). The REFM model uses  
64 the solar wind speed as an input parameter and provides forecasting values of >2MeV  
65 electron fluxes of the 1-3 day ahead. The prediction efficiency of the first day is 0.71, but  
66 that of the next days is poor because the outer radiation belt is rapidly variation in a magnetic  
67 disturbance period (Baker et al., 1990).

68 Based on the wave-particle interaction mechanism, He et al. (2013) takes geomagnetic  
69 pulsation parameters as input parameters, and combines linear filter technology and Kalman  
70 filter to establish the relativistic electrons prediction model at the GEO. The PE of model for  
71 2004 is about 0.73, which is equivalent to the imitation REFM model. But, the prediction  
72 results is lower than other models in 2005, that PE is about 0.62. Potapov et al. (2014, 2016)  
73 combined the mechanisms of radial diffusion and wave-particle interaction to establish a  
74 daily prediction model using a multivariate regression method. This model takes the  
75 amplitude of Pc4-5 oscillation, the maximum for a day fluxes of seed electrons, and the IMF  
76 as input parameters to establish the model. The model is obviously characterized by an  
77 extreme prediction value ahead of the measured value.

78 ULF Pc5 waves can migrate inward to lower L-shells and may accelerate low and medium  
79 energy electrons to relativistic energy via several proposed mechanisms (Simms et al., 2018).  
80 So, the Pc5 wave may be the key to electronic excitation at GEO. There are many studies  
81 show that Pc5 power has a good correlation with relativistic electrons fluxes ( Regi et al.,  
82 2015; Lam, 2017). In this work, we use Pc5 power as one of parameters to predict the >  
83 2MeV electron fluxes.

84 Since the relationship between the relativistic electron fluxes and each parameter is not  
85 completely linear, the variation of relativistic electrons is too complex to describe the  
86 relationship between the input parameters and the output of electron fluxes as a functional

87 relationship. However, the neural network method has good learning ability and represents a  
88 better approach to solve the nonlinear problem. Fukata et al. (2002) and Ling et al. (2010)  
89 established a neural network model to predict the relativistic electron fluxes. The PE of  
90 Fukata's model is approximately 0.6. Ling's model is more efficient than Fukata's, and the  
91 PE of the model is close to 0.7, that of input parameters are the indexes of geomagnetic  
92 disturbance, however, ignored solar wind parameters. For the sudden enhancement and loss  
93 of high-energy electron fluxes, Qian et al. (2020) combined the EMD algorithm and Kalman  
94 filter algorithm to establish the EMD-KLM model for high-energy electron prediction. The  
95 average PE of  $> 2\text{Mev}$  electron fluxes can reach up to 0.8. Especially, the accuracy of  
96 forecast is excellent for the sudden decline of electron fluxes, but the accuracy of forecast  
97 needs to be improved during the sudden jump of electron fluxes.

98 With the development of machine learning, deep learning neural networks are also used in  
99 the prediction of high-energy electron fluxes. Wei et al. (2018) established a prediction  
100 model based on the deep learning algorithm LSTM network, called the LSTM-FRK model.  
101 The prediction efficiency of Wei's model is in the range of 0.65-0.81, and it verifies the good  
102 effectiveness of the LSTM network in predicting high-energy electron fluxes. However, the  
103 model uses historical high-energy electron fluxes, Kp index, and daily average distances  
104 from the magnetosphere to model, which indicates that input parameters need to be further  
105 optimized. In addition, intelligent algorithms, including radial basis functions and support  
106 vector machines, are also used for the prediction of relativistic electrons (Xue & Ye, 2004;  
107 Guo et al., 2013).

108 Although these models have achieved great success in predicting electron fluxes, there is  
109 still much room of improvement for the accuracy of the magnetic storm period and the  
110 prediction of the minimum inflection point of the  $>2\text{MeV}$  electron fluxes. Therefore, using  
111 geomagnetic pulsation parameters and related geomagnetic indexes, we propose a new  
112 combination model, named the EMD-LSTM model, to predict the  $>2\text{MeV}$  electron fluxes  
113 based on the combination of EMD and LSTM network. The EMD-LSTM model can solve  
114 the non-stationary and nonlinear problems of high-energy electron fluxes data, and  
115 geomagnetic pulsation parameters are easier to obtain and more stable than solar wind

116 parameters.

## 117 **2. Data**

### 118 **2.1 Data Source and Processing**

119 In this work, we use a daily value of the  $>2$  MeV electron fluxes in order to eliminate the  
120 local time effects. The fluxes data derives from the relativistic electron fluxes of 5 min time  
121 resolution is obtained from the GOES10 satellite and can be available at the NOAA website  
122 (<https://satdat.ngdc.noaa.gov/sem/goes/data>). The daily Pc5 power datasets derives from  
123 ground magnetic data, which is collected by CANMOS observatories located in the auroral  
124 zone proximal to footprints of field lines, and the detail of the datasets is shown in Table1.  
125 To process the magnetic data, the band pass filter is first used to filter the tiny data to extract  
126 the variation of the Pc5 band. Then, use the Hanning window to calculate the fast Fourier  
127 transform to obtain the Pc5 power spectrum estimation based on the hourly data. Finally, the  
128 hourly power is integrated to obtain daily Pc5 power.

129 **Table1. Coordinates of CANMOS Auroral Zone Observatories**

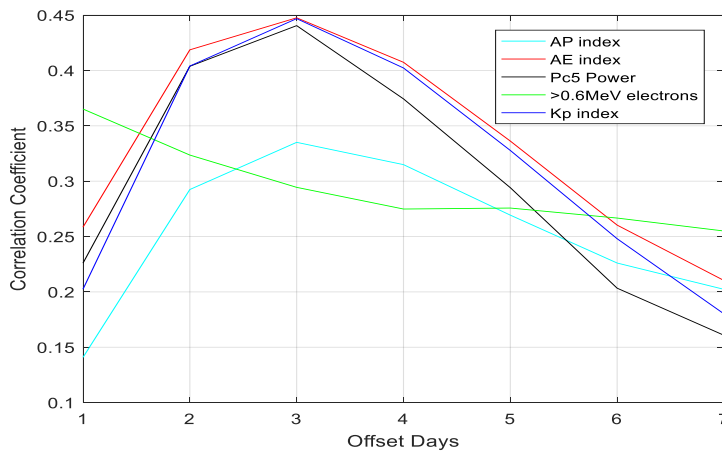
Code	Station	Geographic Latitude	Geographic Longitude	Geomagnetic Latitude	Geomagnetic Longitude	L
FCC	ForChurchill	$58.8^{\circ}N$	$94.1^{\circ}W$	$68.8^{\circ}N$	$94.1^{\circ}W$	8.18

### 130 **2.2 Selection of Input Parameters**

131 The previous studies indicated that Pc5 wave have strong correlation with energy electron  
132 fluxes increase at GEO (O'Brien et al., 2003; Borovsky & Deton, 2014; Regi et al., 2015;  
133 Lam, 2017; Simms et al., 2018). In fact, Simms et al. (2018) suggested that Pc5 waves is the  
134 main waves that drive electron acceleration. Lam (2017) analyzed the relationship between  
135 Pc5 wave and  $>2$ MeV electron fluxes in two solar cycles, and proposed that strong ground  
136 Pc5 is a precursor of enhanced relativistic electron fluxes at GEO by ahead 2-3 days for all  
137 phases. On the other hand, solar wind parameters are usually used in the prediction model of  
138 relativistic electron fluxes. Regi et al. (2015) proposes that the Pc5 power is highly  
139 correlation with solar wind pressure fluctuations and with the solar wind speed by several

140 hours offset. Comparison with solar wind parameters, the Pc5 power is derived from ground  
 141 magnetic data, so it cost lower and is more stable than satellite data. So, we use the Pc5  
 142 power as one of input parameters to predict > 2MeV electron fluxes.

143 In this work, we also use the >0.6 MeV electron fluxes ( Potapov et al., 2016),  
 144 geomagnetic indexes (Ap, Kp, AE) (Yoursfi et al., 2009, Sakaguchi et al., 2013) and the  
 145 historical >2 MeV electron fluxes (X) as other input parameters to predict the >2 MeV  
 146 electron fluxes 1 day ahead. Meanwhile, analyze the correlations between each input  
 147 parameter and >2MeV electron fluxes. The result is shown in Figure1.



148

149 **Figure1 The correlations of between input parameters used and >2MeV electron fluxes.**

150 In Figure1, we can conclude that the best correlation of between each input and  
 151 the >2MeV electron fluxes is 1-3 days ahead. So, the input parameters used in this work is  
 152 shown in Table2.

153

**Table2. The input parameters of the EMD-LSTM model**

Inputs	Correlation coefficient
$Ap(t-3)$	0.33
$AE(t-3)$	0.46
$>0.6MeV(t-1)$	0.36
$Pc5(t-3)$	0.43

---

$Pc5(t-2)$	0.40
$Kp(t-3)$	0.44
$X(t-1)$	0.81

---

154

### 155 **3. Method**

#### 156 **3.1 EMD Algorithm**

157       Due to the external squeeze of the solar wind, the high-energy electrons during a  
158 magnetic storm change very drastically. The non-stationary and nonlinear characteristics of  
159 the  $>2\text{MeV}$  electron fluxes data series is very obvious, which introduces great difficulties to  
160 accurate forecasting. Previous models use statistical methods to deal with the impact of  
161 nonlinear problems on forecast (Xiao et al., 2012), but the non-stationary problem of data  
162 series is not taken seriously. The EMD algorithm is a method that can well deal with the  
163 non-stationarity problem of high-energy electron flux data series, and the basic idea is that  
164 all complex signals are composed of simple eigenmode functions (IMF) (Huang et al.,  
165 1998). These IMF components are arranged in the order of high frequency to low frequency,  
166 where each IMF is independent of each other (Sain & Stephan, 1997). The components of  
167 different scales in the high-energy electron flux data sequence is decomposed one by one  
168 by the EMD algorithm, and several data sequences with different characteristic scales are  
169 generated. These components of different characteristic scales are more regular than the  
170 original high-energy electron flux data sequence, that help to improve the prediction  
171 accuracy. Qian et al. (2020) introduced the EMD algorithm to process and forecast  
172 the  $>2\text{MeV}$  electron fluxes, called the EMD-KLM model, and found that the forecast  
173 results is greatly improved comparison with the prediction result of no the EMD algorithm.

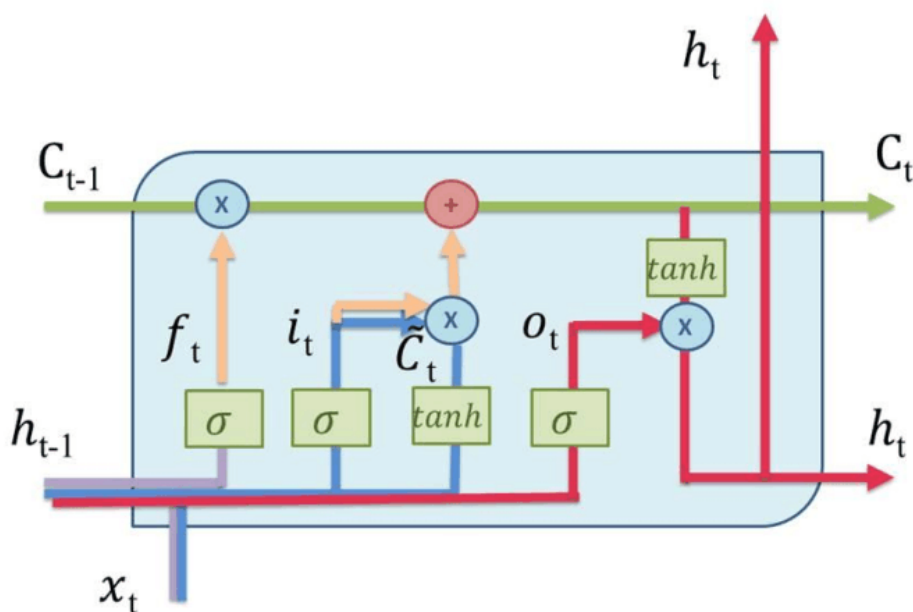
#### 174 **3.2 LSTM Network**

175       The high-energy electron flux usually increases significantly during the recovery phase  
176 of a magnetic storm, and sometimes it suddenly increases by 3-4 orders of magnitude. Most  
177 of the existing forecasting models is difficult to accurately follow the event of sudden increase

178 in high-energy electron fluxes. However, with the development of machine learning (ML),  
179 deep learning neural networks is also used in the prediction of the >2MeV electron fluxes.

180 The LSTM Network is a type of recurrent neural network(RNN). The iterative function  
181 loops is used by RNN to store information (Graves, 2012). They behave as loops, allowing  
182 information to pass from one unit of the network to the next. If this loop is unrolled, the RNN  
183 would be thought as multiple copies of the same network. This feature makes RNN can  
184 remember historical information (Tan et al., 2018). Thus, it is suitable to forecast the >2MeV  
185 electron fluxes during a magnetic storm period.

186 However, if the information needed is too far in the past, the standard RNN is unable to  
187 learn how to connect the information each other. This problem is because of the vanishing  
188 gradient problem occurring during the training phase of RNN (Hochreiter & Schmidhuber,  
189 1990). The LSTM is designed to avoid the vanishing gradient problem, that can remember  
190 information for long periods of time. They have a chain-like structure like RNN, but the  
191 repeating module has a specific structure. Figure 2 shows an LSTM cell. The key of the  
192 LSTM cell is as follows: 1. The cell state, and 2. The cell gate. The cell gate in green on  
193 figure 2 is like a conveyor belt which is connected to gates. Gates can add or remove  
194 information from the cell state depending on information required by the cell. Basically, three  
195 gates are used: an input gate in blue, a forget gate in purple and an output gate in red in Figure  
196 2. The detail algorithm is described in Wei et al. (2018).



198 **Figure 2 LSTM cell of schematic diagram. The cell state is in green, the forget in**  
199 **purple, the input gate in blue, and the output gate in red.**

200 The LSTM network can more easily capture the non-linear relationship in the data set of  
201 high-energy electron flux to predict the >2 MeV electron fluxes more accurately based on the  
202 useful information in the historical data series.

203 Wei et al (2018) used the LSTM network to predict the daily integral values of the  
204 high-energy electron fluxes at GEO for the next day by inputting the historical high-energy  
205 electron flux, the geomagnetic index Kp, and the daily average value of the magnetopause.  
206 And the forecast results is better, which verifies the feasibility of using the LSTM network to  
207 predict the >2 MeV electron fluxes. However, the model can be further improved in the  
208 selection of predictors.

209

### 210 **3.3 EMD-LSTM Model**

211 The LSTM network is effective in dealing with the nonlinear problem of the data  
212 sequences. It has a memory function and can capture more complex nonlinear relationships  
213 in the data sets, which is more suitable for the prediction of the data sequences. At the same  
214 time, the EMD algorithm is very effective in dealing with the non-stationary problem of  
215 high-energy electron flux data series. Therefore, we combine the EMD algorithm and the  
216 LSTM network to predict the >2 MeV electron fluxes at GEO for the first time. The  
217 combined forecast model is named the EMD-LSTM model, which uses ultra-low frequency  
218 Pc5 power as one of input parameters to predict the >2 MeV electron fluxes.

219 Figure 3 shows the main process of the combined forecast. The main steps is as follows:

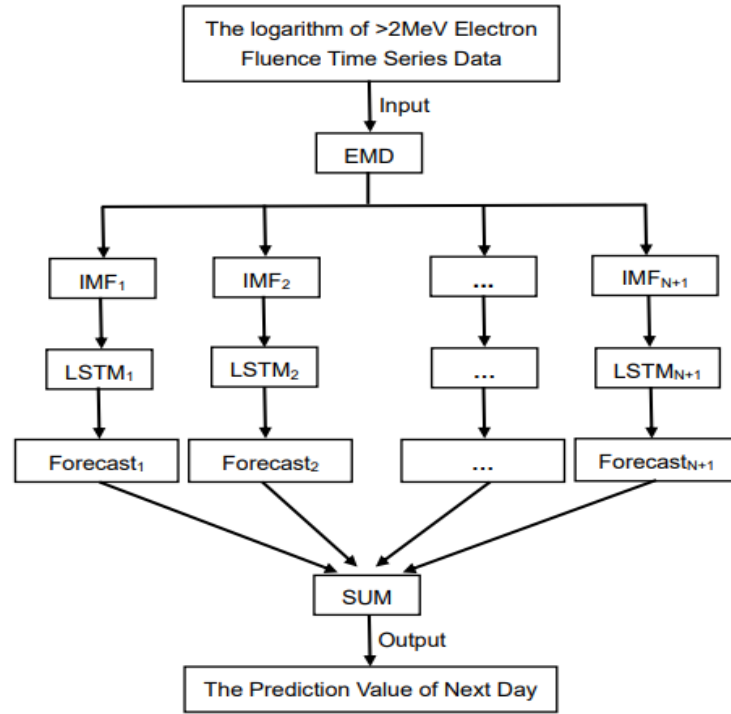
220 (1) Use the EMD algorithm to decompose the observed values of the >2 MeV electron  
221 fluxes to obtain  $n$  IMF components and one margin;

222 (2) Input the prepared predictor into the LSTM network;

223 (3) Use the LSTM network to predict each component and get the predicted value of  
224 each component for the next day;

225 (4) Add the predicted values of  $n$  components to obtain the predicted value of the >  
226 2MeV electron fluxes for the next day;

227 The EMD-LSTM model is a rolling forecast model, so the data sets needs to be  
 228 re-decomposed in advance every day for the next forecast. The time step of the combined  
 229 forecasting model is 3 steps and it means that the daily flux of the >2 MeV electron fluxes for  
 230 the next day is predicted by the historical data of the previous three days.



231

232

**Figure 3 The flow chart of the EMD-LSTM model**

## 233 4. Results and Analysis

### 234 4.1 The Evaluation of Forecasting >2MeV Electron Fluxes

235 In this work, we use three indicators, like Root Mean Square Error( $\sigma$ ), Correlation  
 236 Coefficient (R), and the Prediction Efficiency(PE), to evaluate the performance of the >2  
 237 MeV electron fluxes forecasting. In the experiments, we compare the performance indicators  
 238 of between the EMD-LSTM model and the other classical models. They are defined as  
 239 follows:

$$240 \quad \sigma = \sqrt{\frac{1}{n} \sum_{i=1}^n (f_i - F_i)^2} \quad (1)$$

$$241 \quad R = \frac{\sum_{i=1}^n (f_i - \bar{f})}{\sqrt{\sum_{i=1}^n (f_i - \bar{f})^2 (F_i - \bar{F})^2}} \quad (2)$$

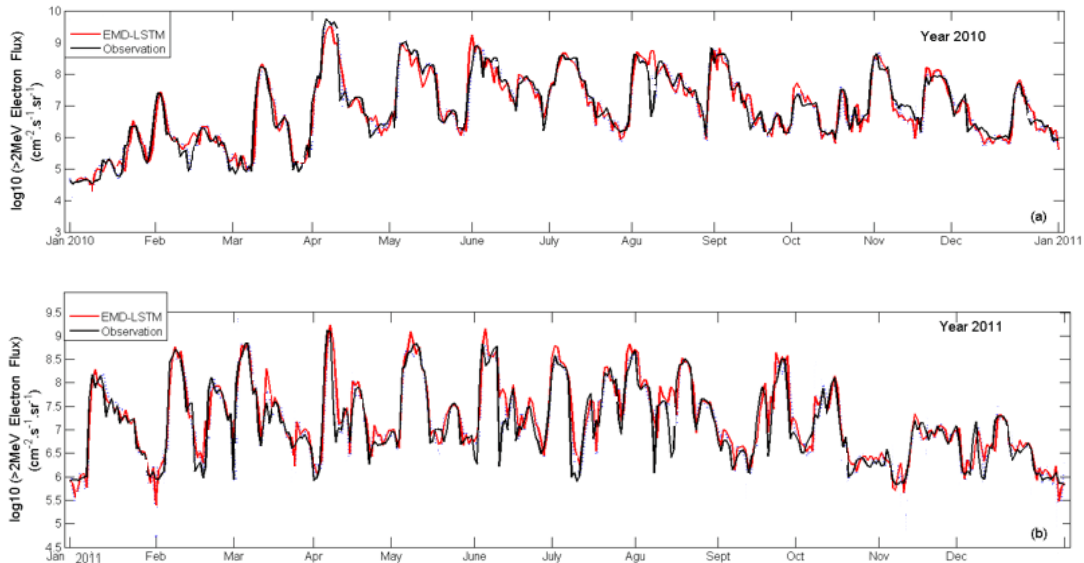
$$PE = \frac{\sum_{i=1}^n (f_i - F_i)^2}{\sum_{i=1}^n (\bar{F} - F_i)^2} \quad (3)$$

242

243 Where  $f_i$  is the forecast value,  $F_i$  is the observation value,  $\bar{f}$  is the mean of the forecast  
 244 value,  $\bar{F}$  is the mean value of the observation, and  $n$  is the number of samples. Each of these  
 245 indicators evaluates the model on a different perspective. The  $\sigma$  indicates error and the R  
 246 indicates the level of fitting between the prediction value and the observation. The PE  
 247 evaluates the accuracy of the prediction of the >2 MeV electron fluxes. As such, the smaller  
 248  $\sigma$ , the larger R and PE, are the better the prediction performance. We compare the  $\sigma$ , R and  
 249 PE of predicting the >2MeV electron fluxes by between the EMD-LSTM and the classical  
 250 models in the next section.

#### 251 4.2 The Prediction Results of the EMD-LSTM model

252 In this work, the data series of the >2MeV electron fluxes from 2001 to 2009 is used by  
 253 the training set, and the electron fluxes from 2010 to 2013 is used by the test set. We use the  
 254 seven parameters selected as the inputs of the EMD-LSTM model. Figure 4 shows the  
 255 prediction results of the EMD-LSTM model during from January 2010 to December 2011  
 256 (The red line represents the prediction value of the EMD-LSTM model and the black line  
 257 represents the observation of the >2MeV electron fluxes). The forecast value of the  
 258 EMD-LSTM model is close to the observation of the >2MeV electron fluxes. It is worth  
 259 noting that the amount of  $\log_{10}$ (electron fluxes) is even up to 8-9, the prediction values of the  
 260 EMD-LSTM model is still close to the observations. There are two main reasons. Firstly,  
 261 when the amount of  $\log_{10}$ (electron fluxes) is up to 8 or 9, it is often caused by the sudden  
 262 acceleration of relativistic electrons which is often related to the pc5 wave (Mathie & Mann,  
 263 2000; Lam, 2017). So, in this work, we used the pc5 as one of input parameters, and the  
 264 prediction results is ideal. Secondly, the LSTM network could capture the historical  
 265 information to process nonlinear problems of data series, and the EMD algorithm could  
 266 reduce the influence of non-stationary of data series (Qian et al., 2020). Therefore, even if the  
 267 high-energy electron fluxes changes suddenly, the EMD-LSTM model can also fit the >2  
 268 MeV electron fluxes well.



269

270

271 **Figure 4 The comparison of the EMD-LSTM prediction values with the observations**  
 272 **from Jan 2010 to Dec 2011.**

273 Compared with the data sequences of the  $>2$  MeV electron fluxes in 2010, the  $>2$  MeV  
 274 electron flux data series changes more dramatically in 2011, so the levels of non-stationary  
 275 and non-linearity are significantly enhanced. The EMD-LSTM model combines the EMD  
 276 algorithm effectively process the non-stationary problem of data series, with the LSTM  
 277 network improves the ability of the model to deal with nonlinear problems. Comparison with  
 278 the standard RNN can only remember information in a short period, the LSTM network can  
 279 remember data information within a long time, and captures useful information of training set  
 280 to predict the  $>2$  MeV electron fluxes of 1 day ahead. The LSTM network can record the  
 281 characteristics of the changes of the  $>2$  MeV electron fluxes during the historical high-energy  
 282 electron storms and retains the useful information. Therefore, the LSTM network can deal  
 283 with sudden change of the relativistic electron fluxes events. Figure 4 shows that the  
 284 EMD-LSTM model can also fit actual observation of the  $>2$  MeV electron fluxes reaching  
 285 peak values during the high-energy electron flux storm. In the actual operation, the sudden  
 286 enhancement of the high-energy electron fluxes should be paid more attention to forecast, to  
 287 minimize the loss by protection measures taken to the satellite equipment.

288 **Table 3. the comparison of PE,  $\sigma$  and R between the EMD-LSTM and other models**

Year	Model	PE	$\sigma$	R
------	-------	----	----------	---

2010	LSTM	0.89	0.37	0.94
	EMD-KLM	0.88	0.35	0.93
	EMD-LSTM	0.92	0.32	0.96
2011	LSTM	0.75	0.39	0.88
	EMD-KLM	0.77	0.41	0.89
	EMD-LSTM	0.81	0.37	0.90
2012	LSTM	0.77	0.38	0.88
	EMD-KLM	0.79	0.39	0.89
	EMD-LSTM	0.84	0.33	0.92
2013	LSTM	0.79	0.37	0.89
	EMD-KLM	0.78	0.37	0.90
	EMD-LSTM	0.83	0.34	0.92

289 Table 3 shows the comparison of the EMD-LSTM model with the LSTM model and the  
290 EMD-KLM model (Qian et al., 2020) based on the same datasets. The results in Table  
291 3 indicates that the effectiveness of the EMD-LSTM model is greatly improved compared  
292 with the other two models, on the basis of the performance indicators of PE,  $\sigma$  and R. The  
293 data series of non-stationary and nonlinear characteristics are more obvious, which derive  
294 from the high-energy electron flux storms frequently occurs during from 2011 to 2013  
295 especially (Qian et al., 2020). The PE of the EMD-KLM model is comparable to that of the  
296 LSTM model. Further more, the EMD-LSTM model, combined the EMD algorithm and the  
297 LSTM network, has a certain improvement in the PE compared with the other two models.  
298 This also fully shows that the EMD-LSTM model can deal with the effects of non-stationary  
299 and nonlinear characteristics, which derives from magnetic storms resulting in drastic  
300 fluctuations of the high-energy electron flux data series.

301 **Table 4. the comparison of PE between the EMD-LSTM and the previous classical**  
302 **models in the period of 2003-2006**

Model/Year	2003-2004	2005-2006
NICT(PE)	0.72	0.79
Low-energy(PE)	0.66	0.74

RDF(PE)	0.64	0.75
LSTM-FRK(PE)	0.74	0.81
EMD-LSTM(PE)	0.79	0.83

303 Table 4 shows the PE comparison of between the EMD-LSTM model and the previous  
304 classical models. It is indicates that the PEs of the EMD-LSTM model is higher than that of  
305 those models in the period of 2003-2006. Specially, the improvement of PE in 2003-2004 is  
306 the most obvious. There are 13 high-energy electron flux storm events occurred in 2003-2004,  
307 more than double times in 2005-2006. Therefore, the variation of the >2 MeV electron fluxes  
308 in 2003-2004 is more drastic, and the level of non-stationary and nonlinear of the data series  
309 is significantly enhanced. So, the PEs of all prediction models in 2003- 2004 is lower than  
310 that in 2005-2006. The EMD-LSTM model can deal with the non-stationary and nonlinear  
311 problems of data series well by the improvement of mathematical method. Therefore, even in  
312 the year with strong non-stationary and nonlinear level, the EMD-LSTM model can also  
313 achieve better PE performance. In addition, the most of models (Li et al., 2001; Turner and Li,  
314 2008; Wei et al., 2018) in Table 4, used solar wind as input parameters, but the EMD-LSTM  
315 model uses Pc5 and related geomagnetic indexes to forecast the >2 MeV electron fluxes . On  
316 the basis of the experimental results, it is found that geomagnetic pulsation parameters can  
317 also achieve a better forecast effect as a forecasting factor of the model. The prediction results  
318 of the EMD-LSTM model also verify the feasibility of geomagnetic pulsation parameter as a  
319 predictor of high-energy electron fluxes.

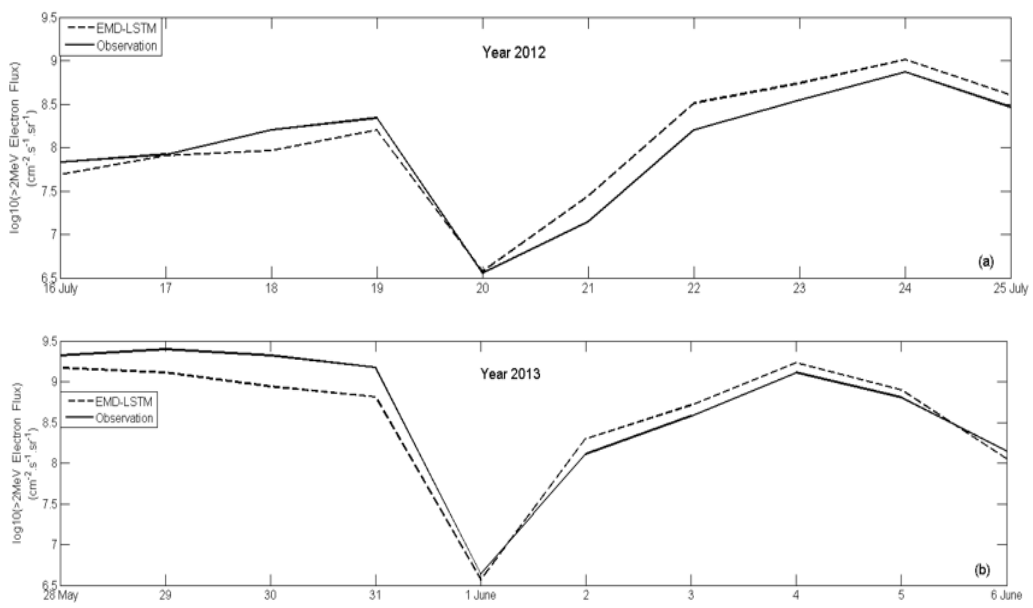
### 320 **4.3 Analysis of the >2 MeV Electron Fluxes During Magnetic Storms**

321 During a geomagnetic storm, the high-energy electron fluxes changes dramatically, so the  
322 accurate prediction of the >2 MeV electron fluxes is very important to protect for satellite  
323 instruments to reduce the risk of damage. Here, two cases of the high-energy electron flux  
324 storm, during from 16 July to 25 July 2012 and from 28 May to 6 June 2013, are chose to  
325 analysis. The prediction results is illustrated in Figure 5. During an initial phase of magnetic  
326 storm, the >2 MeV electron fluxes will decrease greatly and then rise rapidly, which is  
327 consistent with the variation characteristics of the general electron flux storms. Specially, the  
328 extreme points of the data series, on 20 July 2012 and 1 June 2013, are very important to the

329 prediction, which indicate the high-energy electron fluxes begins to rapidly enhance. As can  
330 be seen in Figure 5, the prediction values of the EMD-LSTM model is consistent with the  
331 observation of the  $>2$  MeV electron fluxes, and particularly the prediction values coincide  
332 with the observation values at the extreme points, few time offset.

333 There are two reasons for highly effective in prediction. Firstly, the EMD algorithm greatly  
334 reduces the non-stationary problem caused by the drastic changes of the high-electron fluxes  
335 (Qian, et al., 2020). Secondly, the LSTM network can remember the variation characteristics  
336 of the high-energy electron storm events in the training set and extract the relevant  
337 information (Wei et al., 2018). Therefore, when the high-energy electrons suddenly drop, the  
338 LSTM network can accurately predict the subsequent values of the  $>2$  MeV electron fluxes,  
339 based on the analysis of the information of the training set samples. This is very important in  
340 practical forecasting, to accurately predict the start time of high-energy electron storm and  
341 provide immediate protection for satellite equipment.

342



343

344

345 **Figure 5. The comparison of the EMD-LSTM model prediction with the observations**  
346 **during energy electron storm events**

### 347 **5. Conclusion**

348 In this paper, we combine the EMD algorithm and the LSTM network to construct the  
349 EMD-LSTM model to predict the  $> 2\text{MeV}$  electron fluxes at GEO. The EMD-LSTM model  
350 can deal with the non-stationary and nonlinear of data series, and the effectiveness of the

351 model is improved compared with other classical models.

352 The prediction results of the EMD-LSTM model is excellent during the high-energy  
353 electron fluxes storm, and particularly the extreme points of the >2 MeV electron fluxes data  
354 series is accurately predicted, and few time offset.

355 Pc5 and related geomagnetic indexes are used to predict the > 2MeV electron fluxes. The  
356 experimental results verify that the parameters of ground can achieve a better forecast effect  
357 as a forecasting factor of the model, and those data acquisition of parameters is stable and  
358 lower cost.

359 **Acknowledgments:** This work was supported by the National Key R&D Program of China  
360 (2018YFF01013706), the Natural Science Foundation of Jiangsu Province (BK20170952),  
361 the National Natural Science Foundation of China grant (No.41874190, 42074183, 61572015),  
362 and the Stable support projects of institutes for basic scientific research (A131901W14). The  
363 author acknowledges National Oceanic and Atmospheric Administration(NOAA), NASA  
364 OMNI database and the Word Data center for Geomagnetism, Kyoto for providing the  
365 observation data.

366 **Data Availability Statement:**

367 The high-energy electron fluxes observations originates from the GOES satellite on the  
368 website of NOAA (<https://satdat.ngdc.noaa.gov/sem/goes/data>). Geomagnetic indexes come  
369 from the world geomagnetic data center of the Memanbetsu station in Japan  
370 (<http://swdcwww.kugi.kyoto-u.ac.jp/wdc/Sec3.html>). The daily Pc5 power datasets derives  
371 from ground magnetic data, which is collected by CANMOS observatories.

372

## 373 **References**

374 Baker, D. N., Mcpherron, R. L., Cayton, T. E., & Klebesadel, R. W. (1990). Linear prediction  
375 filter analysis of relativistic electron properties at 6.6 RE. *Journal of Geophysical Research:*  
376 *Space Physics*, 95, 15133-15140. <https://doi.org/10.1029/JA095iA09p15133>.

377 Borovsky, J. E., & Denton M. H. (2014). Exploring the cross correlations and autocorrelations  
378 of the ULF indices and incorporating the ULF indices into the systems science of the solar  
379 wind-driven magnetosphere. *Journal of Geophysical Research: Space Physics*, 119, 4307  
380 -4334. doi:10.1002/2014JA019876.

381 Futaka, M., Taguchi, S., Okuzawa, T., & Obara, T. (2002). Neural network prediction of  
382 relativistic electrons at geosynchronous orbit during the storm recovery phase: effects of  
383 recurring substorms. *Annales Geophysicae*, 20, 947-951. doi: 10.5194/angeo-20-947-2002.

384 Graves, A. (2012). Long Short-Term Memory. Springer Berlin Heidelberg, 37-45. doi: 10.1007/978-3-642-24797-2\_4.

386 Guo, C., Xue, B. S., & Lin, Z. X. (2013). Geosynchronous orbit high energy electron flux  
387 prediction method. *Chinese Journal of space science*, 33 (4), 418-426.

388 He, T., Liu, S. Q., Shen, H., & Gong, J. C. (2013). Quantitative prediction of relativistic  
389 electron flux at geosynchronous orbit with geomagnetic pulsations parameters. *Chinese*  
390 *Journal of space science*, 33(1), 20-27.

391 Hochreiter, S., & Schmidhuber, J. (1997). Long Short-Term Memory. *Neural Computation*,  
392 9(8), 1735-1780. doi:10.1162/neco.1997.9.8.1735.

393 Huang, N. E., Shen, Z., & Long, S. R. (1998). The empirical mode decomposition and the  
394 Hilbert spectrum for nonlinear and non-stationary time series analysis. *Proceedings of The*  
395 *Royal Society of London A: Mathematical, Physical and Engineering Sciences*,  
396 454(1971):903-995. <https://doi.org/10.1098/rspa.1998.0193>.

397 Lam, H.-L. (2017). On the predictive potential of Pc5 ULF waves to forecast relativistic  
398 electrons based on their relationships over two solar cycles. *Space Weather*, 15, 163-179.  
399 doi:10.1002/2016SW001492.

400 Li, X., Termerin, M., Baker, D. N., Reeves, G. D., & Larson, D. (2001). Quantitative  
401 prediction of radiation belt electrons at geostationary orbit based on solar wind  
402 measurements. *Geophysical Research Letters*, 28(9). [https://doi.org/10.1029/2000GL0126](https://doi.org/10.1029/2000GL012681)  
403 81.

404 Ling, A. G., Ginet G. P., Hilmer, R. V., & Perry, K. L. (2010). A neural network-based  
405 geosynchronous relativistic electron flux forecasting model. *Space Weather*, 8, S09003.  
406 doi:10.1029/2010SW000576.

407 Mathie, R. A., & Mann, I. R. (2000). A correlation between extended intervals of ULF wave  
408 power and storm-time geosynchronous relativistic electron flux enhancements.  
409 *Geophysical Research Letters*, 27(20), 3261-3264. doi:10.1029/2000GL003822.

410 O'Brien, T. P., Lorentzen, K. R., Man, I. R., Meredith, N. P., Blake, J. B., Fennell, J. F.,

411 Looper, M. D., Milling, D. K., & Anderson, R. R. (2003). Energization of relativistic  
412 electrons in the presence of ULF power and MeV microbursts: Evidence for dual ULF  
413 and VLF acceleration. *Journal of Geophysical Research*, 108(A8), 1329. doi:10.1029/2002J  
414 A009784.

415 Potapov, A., Ryzhakova, L., & Tsegmed, B. (2016). A new approach to predict and estimate  
416 enhancements of “killer” electron flux at geosynchronous orbit. *Acta Astronautica*, 126,  
417 47-51. <http://dx.doi.org/10.1016/j.actaastro.2016.04.017>.

418 Potapov, A., Tsegmed, B., & Ryzhakova, L. (2014). Solar cycle variation of “killer” electrons  
419 at geosynchronous orbit and electron flux correlation with the solar wind parameters and  
420 ULF waves intensity. *Acta Astronautica*, 93, 55–63. [https://doi.org/10.1016/j.actaastro.](https://doi.org/10.1016/j.actaastro.2013.07.004)  
421 2013.07.004.

422 Qian, Y. D., Yang, J. W., Zhang, H., Shen, C. & Wu, Y. (2020). An hourly prediction model of  
423 relativistic electrons based on empirical model decomposition. *Space Weather*, 17,  
424 e2018SW0022078. <https://doi.org/10.1029/2018SW0022078>.

425 Regi, M., Lauretis, M., & Francia, P. (2015). Pc5 geomagnetic fluctuations in response to  
426 solar wind excitation and their relationship with relativistic electron fluxes in the outer  
427 radiation belt. *Earth, Planets and Space*, 67, 1-9. <http://doi.org/10.1186/s40623-015-0180-8>.

428 Sain, & Stephan, R. (1997). The nature of statistical learning theory. *Technometrics*,  
429 38(4),409-422. doi:10.1080/00401706.1996.10484565.

430 Sakaguchi, K., Miyoshi, Y., Satio, S., Nagatsuma, T., Seki, K., & Murata, K. T. (2013).  
431 Relativistic electron flux forecast at geostationary orbit using Kalman filter based on a  
432 multivariate autoregressive model. *Space Weather*, 11, 79-89. doi:10.1002/swe.20020.

433 Simms, L., Engebretson, M., Clilverd, M., Rodger, C., Lessard, M., Gjerloev, J., & Reeves, G.  
434 (2018). A distributed lag Autoregressive model of geostationary relativistic electron fluxes:  
435 comparing the influences of waves, seed and source electrons and solar wind inputs.  
436 *Journal of Geophysical Research:Space Physics*, 123, 3646-3671. [https://doi.](https://doi.org/10.1029/2017JA025002)  
437 [org/10.1029/2017JA025002](https://doi.org/10.1029/2017JA025002).

438 Tan, Y., Hu, Q., Wang, Z., & Zhong, Q. (2018). Geomagnetic index Kp forecasting with  
439 LSTM. *Space Weather*, 16, 406-416. <https://doi.org/10.1002/2017SW001764>.

440 Turner, D. L., & Li, X. (2008). Quantitative forecast of relativistic electron flux at

441 geosynchronous orbit based on low-energy electron flux. *Space Weather*, 6, S05005.  
442 doi:10.1029/2007SW000354.

443 Wei, L., Zhong, Q., Lin, R., Wang, J., Liu, S., & Cao, Y. (2018). Quantitative prediction of  
444 high-energy electron integral flux at geostationary orbit based on deep learning. *Space*  
445 *Weather*, 16, 903–916. <https://doi.org/10.1029/2018SW001829>.

446 Wrenn, G. L., Rodgers, D. J., & Ryden, K. A. (2002). A solar cycle of spacecraft anomalies  
447 due to internal charging. *Annales Geophysicae*, 20, 953-956. [https://doi.org/10.5194/a](https://doi.org/10.5194/angeo-20-953-2002)  
448 [ngeo-20-953-2002](https://doi.org/10.5194/angeo-20-953-2002).

449 Xiao, F. L., Zhang, S., Su, Z., He, Z., & Tang, L. (2012). Rapid acceleration of radiation belt  
450 energetic electrons by Z-mode waves. *Geophysical Research Letters*, 39, L03103.  
451 doi:10.1029/2011GL050625.

452 Xue, B. S., & Ye, Z. (2004). Method for forecasting relativistic electron enhancement events  
453 in geosynchronous orbit. *Chinese Journal of Space Science*, 24 (4), 283-288.

454 Yousrifi, M. R., Kasmaei, B. S., Vahabie, A., Lucas, C., & Araabi, B. N. (2009). Input selection  
455 based on information theory for constructing predictor models of solar and geomagnetic  
456 activity indices. *Solar Physics*, 258(2), 297-318. <https://doi.org/10.1007/s11207-009--941>  
457 8-6.

458

459

460

461

462

463

464

465

466

467

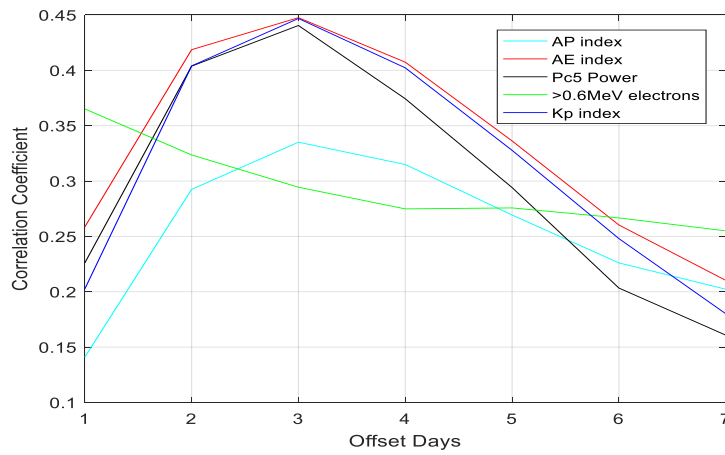
468

469

470

471

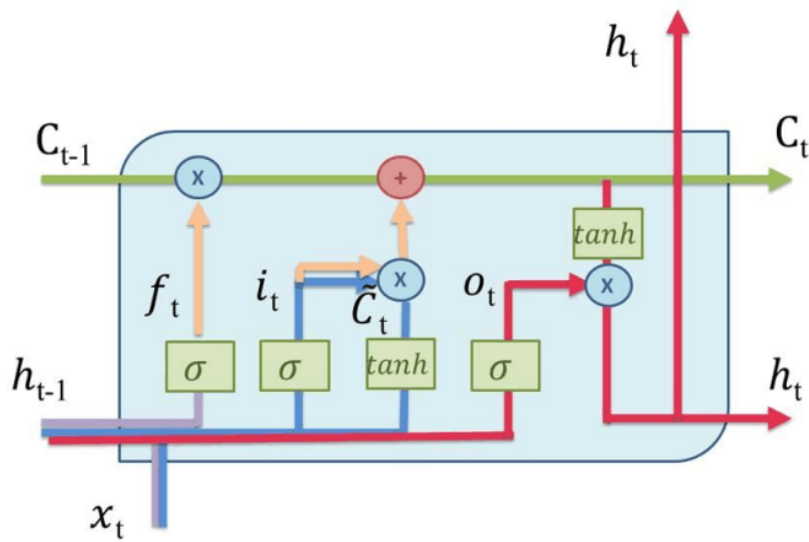
472



473

474

Figure1. The correlations of between input parameters used and >2MeV electron fluxes.

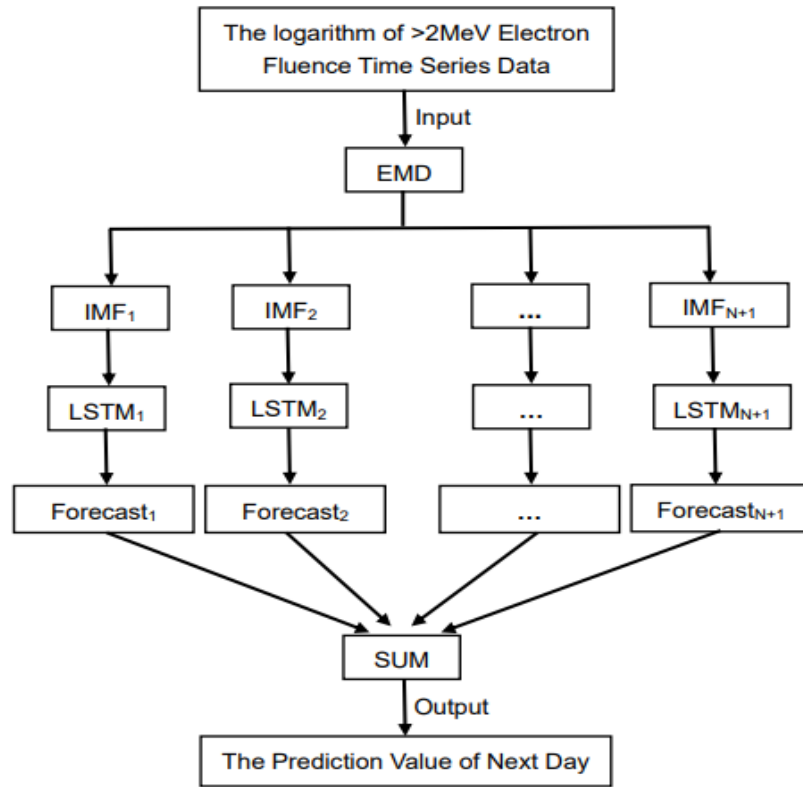


475

476

477

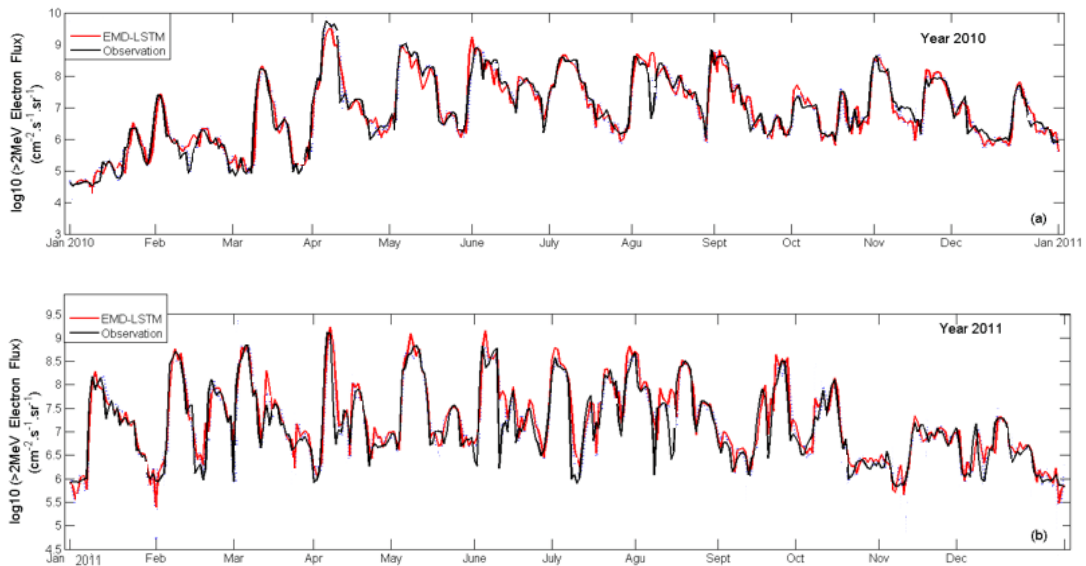
Figure 2. LSTM cell of schematic diagram. The cell state is in green, the forget in purple, the input gate in blue, and the output gate in red.



478

479

Figure 3. The flow chart of the EMD-LSTM model



480

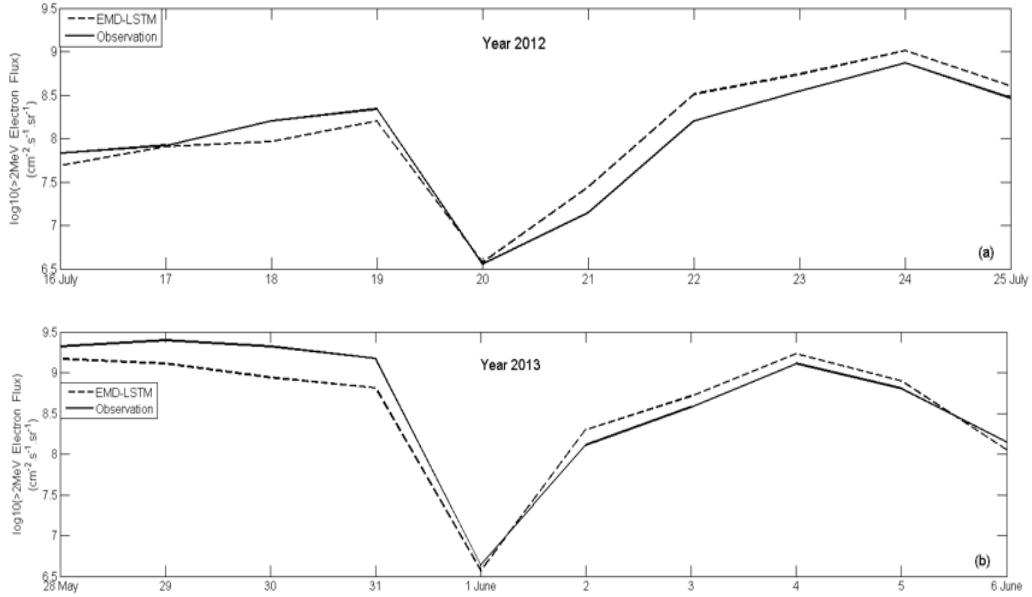
481

482

Figure 4. The comparison of the EMD-LSTM prediction values with the observations from

483

Jan 2010 to Dec 2011.



484

485

486

487

488

489

Figure 5. The comparison of the EMD-LSTM model prediction with the observations during energy electron storm events.

Table1. Coordinates of CANMOS Auroral Zone Observatories.

Code	Station	Geographic Latitude	Geographic Longitud	Geomagnetic Latitude	Geomagnetic Longitude	L
FCC	ForChurchill	58.8° N	94.1° W	68.8° N	94.1° W	8.18

490

491

Table2. The input parameters of the EMD-LSTM model.

Inputs	Correlation coefficient
$Ap(t-3)$	0.33
$AE(t-3)$	0.46
$> 0.6MeV(t-1)$	0.36
$Pc5(t-3)$	0.43
$Pc5(t-2)$	0.40

$Kp(t-3)$	0.44
$X(t-1)$	0.81

492

493 Table 3. the comparison of PE,  $\sigma$  and R between the EMD-LSTM and other models.

Year	Model	PE	$\sigma$	R
2010	LSTM	0.89	0.37	0.94
	EMD-KLM	0.88	0.35	0.93
	EMD-LSTM	0.92	0.32	0.96
2011	LSTM	0.75	0.39	0.88
	EMD-KLM	0.77	0.41	0.89
	EMD-LSTM	0.81	0.37	0.90
2012	LSTM	0.77	0.38	0.88
	EMD-KLM	0.79	0.39	0.89
	EMD-LSTM	0.84	0.33	0.92
2013	LSTM	0.79	0.37	0.89
	EMD-KLM	0.78	0.37	0.90
	EMD-LSTM	0.83	0.34	0.92

494 Table 4. the comparison of PE between the EMD-LSTM and the previous classical models in  
 495 the period of 2003-2006.

Model/Year	2003-2004	2005-2006
NICT(PE)	0.72	0.79
Low-energy(PE)	0.66	0.74
RDF(PE)	0.64	0.75
LSTM-FRK(PE)	0.74	0.81
EMD-LSTM(PE)	0.79	0.83

496